

Estimating Rupture Directions from Local Earthquake Data Using the IPOC Observatory in Northern Chile

by J. Folesky, J. Kummerow, G. Asch, B. Schurr, Ch. Sippl, F. Tilmann, and S. A. Shapiro

ABSTRACT

Local seismic broadband recordings of the Integrated Plate boundary Observatory Chile (IPOC) are used to determine rupture directions for 60 $M \geq 5.0$ events in the foreshock and aftershock series of the 2014 M_w 8.1 Iquique earthquake in northern Chile. The applied method is based on accurate measurements of the P -wave coda polarization, which exhibits systematic, azimuth-dependent variations with time as the earthquake rupture propagates. We demonstrate a general consistency with observations from teleseismic backprojection studies for the main event and its largest foreshock (M_w 6.7) and aftershock (M_w 7.6). A large portion of the here analyzed events show unilateral rupture behavior, with a predominance of down-dip (east) oriented directivity.

This study documents the potential of retrieving rupture directions for $M \sim 5$ earthquakes from a high-quality local seismic monitoring system.

Electronic Supplement: Figures visualizing two processing steps of selection and correction of back azimuths and illustrating the range of different qualities in which the polarization-based rupture tracking can result, and table providing rupture origin times, locations, and magnitudes used in this study.

INTRODUCTION

Motivated by the impendence of a megathrust earthquake in the well-documented northern Chile–southern Peru seismic gap (Comte and Pardo, 1991), the Integrated Plate boundary Observatory Chile (IPOC) has been installed in an international initiative since 2006 (IPOC, 2006; see Fig. 1). It today comprises 21 seismic broadband stations, which are carefully installed in caverns and record continuously at a sample rate of 100 Hz and therefore provide excellent data quality.

The network was in large part functional, when the M_w 8.1 Iquique megathrust earthquake partially broke the seis-

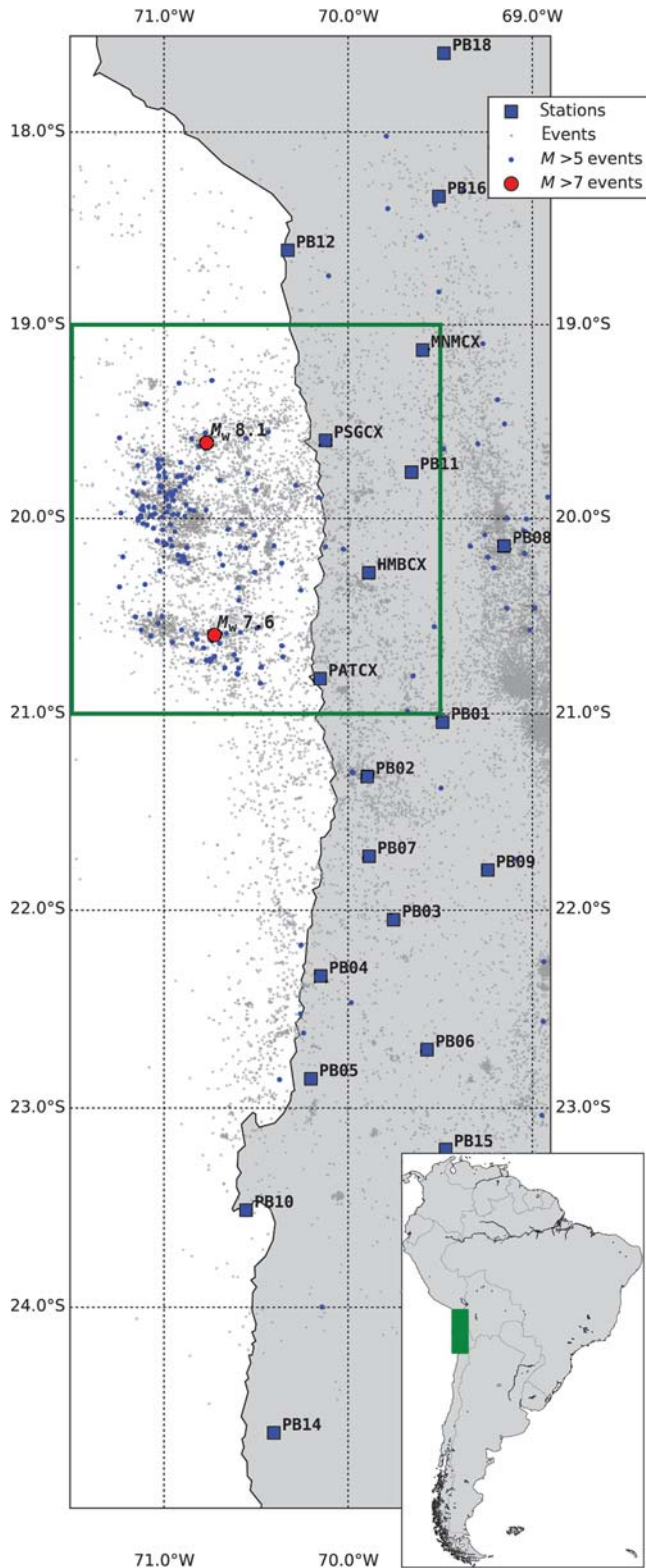
mic gap on 1 April 2014. The mainshock was preceded by exceptionally high foreshock activity, including an M_w 6.7 earthquake two weeks before the mainshock, and followed by intense aftershock seismicity. Several studies used the IPOC network to examine the associated seismicity comprehensively (e.g., Bürgmann, 2014; Hayes *et al.*, 2014; Kato and Nakagawa, 2014; Ruiz *et al.*, 2014; Schurr *et al.*, 2014; Socquet *et al.*, 2017).

The richness of the seismic sequence related to the M_w 8.1 Iquique earthquake and the availability of a high-performance local monitoring system provide an excellent base to study in detail source properties of subduction earthquakes. Here, we test the feasibility to track the rupture propagation of earthquakes using the local IPOC seismic data. The rupture of large earthquakes is nowadays routinely imaged by backprojection of the radiated seismic energy, which is recorded by an array of seismic stations at teleseismic distances (e.g., Ishii *et al.*, 2005; Krüger and Ohrnberger, 2005). Application of this method, however, is usually restricted to earthquakes with magnitudes larger than $M \gtrsim 6.5$. We use a polarization-based method applied to local data here and hypothesize that this approach extends to smaller magnitude events and enables to resolve their rupture directions at higher detail.

Knowledge of the rupture direction has important implications not only for better understanding of the earthquake process itself but also for hazard assessment because ground motion may be strongly affected by the directivity effect (e.g., Calderoni *et al.*, 2015; Tinti *et al.*, 2016).

DATA

We use the seismic broadband of the IPOC. The network extends over a length of about 700 km between 17.6° and 24.6° S (Fig. 1). 100 Hz, three-component waveform data were accessed by the European Integrated Data Archive webservice of GFZ Potsdam (Bianchi *et al.*, 2015). Data were selected from the event catalog by Sippl and Schurr (2017), which



▲ **Figure 1.** Location of the Integrated Plate boundary Observatory Chile (IPOC) stations and earthquake hypocenters in the years 2013 and 2014. The green rectangle borders the study area with 7228 located events. The 146 events with $M \geq 5.0$ used in this study are marked in blue. Red circles indicate the hypocenters of the 2014 M_w 8.1 Iquique mainshock and the M_w 7.6 aftershock.

consists of more than 100,000 double-difference relocated events. We focus our analysis on the foreshock and aftershock seismicity of the 2014 M_w 8.1 Iquique earthquake over a period of the 2 yrs, 2013 and 2014. The study area encloses the 2014 M_w 8.1 megathrust rupture area (19.0° – 21.0° S, 69.5° – 71.5° W). The geographical boundaries ensure that only events in the seismogenic zone between 10 and 65 km depth are considered. The seismicity occurs mainly on the interface with some additional events in the overlying continental crust, and some seismicity originating in a second seismically active deeper band, located 20–25 km below the plate interface between the subducting oceanic Nazca plate and the overlying South American plate.

METHOD

Although coherency of waveforms and of their envelopes is high for seismic arrays located at teleseismic distances from the source and thus facilitates the application of the amplitude stacking based backprojection imaging (e.g., Ishii *et al.*, 2005), the waveforms recorded at distributed stations of a local monitoring system are generally quite variable, due to the radiation pattern, the higher frequencies and local heterogeneity of the seismic velocity, and attenuation structure.

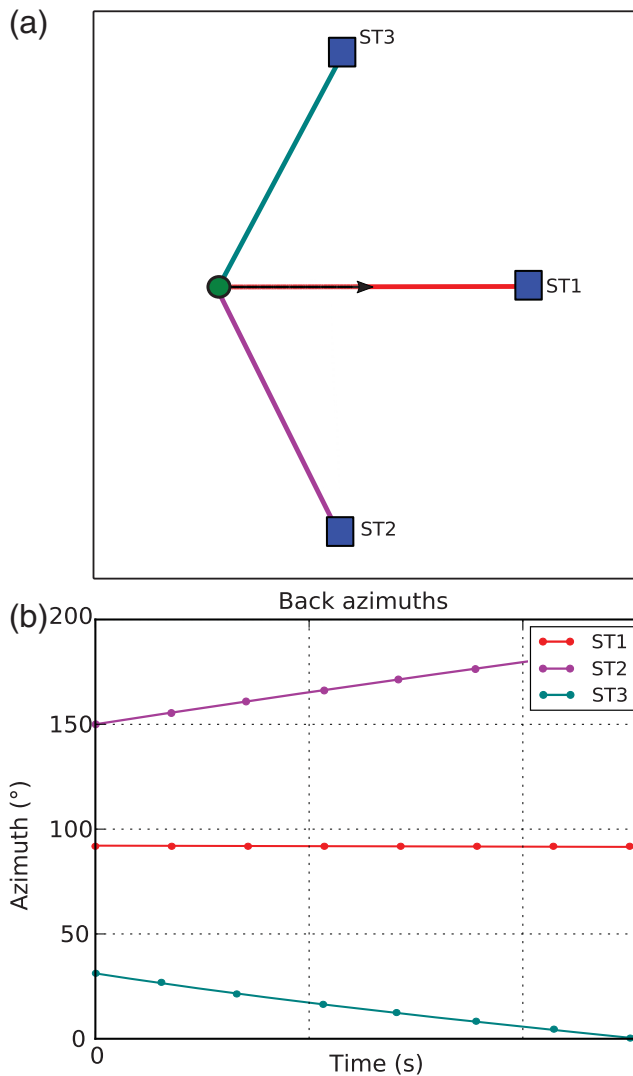
We avoid this complexity here and use a different and simpler geometric method. We follow the approach by Bayer *et al.* (2012), which measures the P -wave polarization at different back azimuths from the source and tracks the variations of the measured polarization directions when the rupture front moves along the rupture surface. The feasibility of the method was originally demonstrated for two large megathrust events, the 2004 M_w 9.3 Sumatra–Andaman earthquake and the 2008 M_w 8.0 Wenchuan earthquake (Bayer *et al.*, 2012), both using regional phases at 10° – 30° distances, and also tested later at reservoir scale (Folesky *et al.*, 2013).

The idea of the procedure is schematically illustrated in Figure 2. Here, the eastward breaking rupture is observed at three stations. At P -onset time, all polarization vectors point toward the event hypocenter and, assuming a homogeneous velocity model, the corresponding ray paths are straight lines and intersect at the hypocenter. For the next timestep, the rupture propagated and the radiated P -wave energy is measured at slightly different back azimuths. Also for this timestep, the rays intersect at one single point along the rupture. In this way, the rupture propagation can be traced.

Mathematically, the minimum of the following function E is determined for each timestep t after the P -onset time

$$E(x, y, t) = \sum_{i=1}^{n_{\text{station}}} d_i^2(x, y, t) \times l_i^2(t) \quad (1)$$

(Bayer *et al.*, 2012), in which $d_i(x, y, t)$ is the shortest distance between the back-azimuthal direction at station i for time t after P onset and the grid point (x, y) (x and y are the longitude and latitude values, respectively). $l_i(t)$ is the linearity of the particle motion for the given time and works as a weighting



▲ **Figure 2.** Sketch of the P -wave polarization-based method. (a) A hypothetical eastward-rupturing event (large green circle for the hypocenter, black arrow for the rupture) is observed at three stations with different back azimuths (thick lines). The azimuth estimates are plotted in (b) for consecutive timesteps (colored circles). Note the opposite trends in the top and bottom curves of stations ST2 and ST3, respectively. As a result of the eastward rupture propagation: an increase of back-azimuth values for station ST2 and a decrease for station ST3 is observed. Angles at stations are measured clockwise from north, projected to the interval $0^\circ \leq \theta \leq 180^\circ$. ST1 shows a constant back azimuth due to the rupture orientation exactly toward the station.

factor ($0 \leq l_i \leq 1$). The temporal migration of the minimum of E represents the progressing rupture front. The smaller the value of E_{\min} , the better is the consistency of the measured back-azimuth estimates. In this study, the depth is fixed to the localization depth and the rupture propagation is resolved only in the horizontal plane.

The P -phase polarization is determined by covariance matrix analysis (e.g., Jurkevics, 1988; Rentsch *et al.*, 2006). For a single station, the covariance matrix analysis yields estimates for

back azimuth, dip, and wavefield linearity from a predefined time window from the three-component seismogram. This time window is moved along the P -wave coda to obtain the estimates for each timestep.

METHOD: EXAMPLE

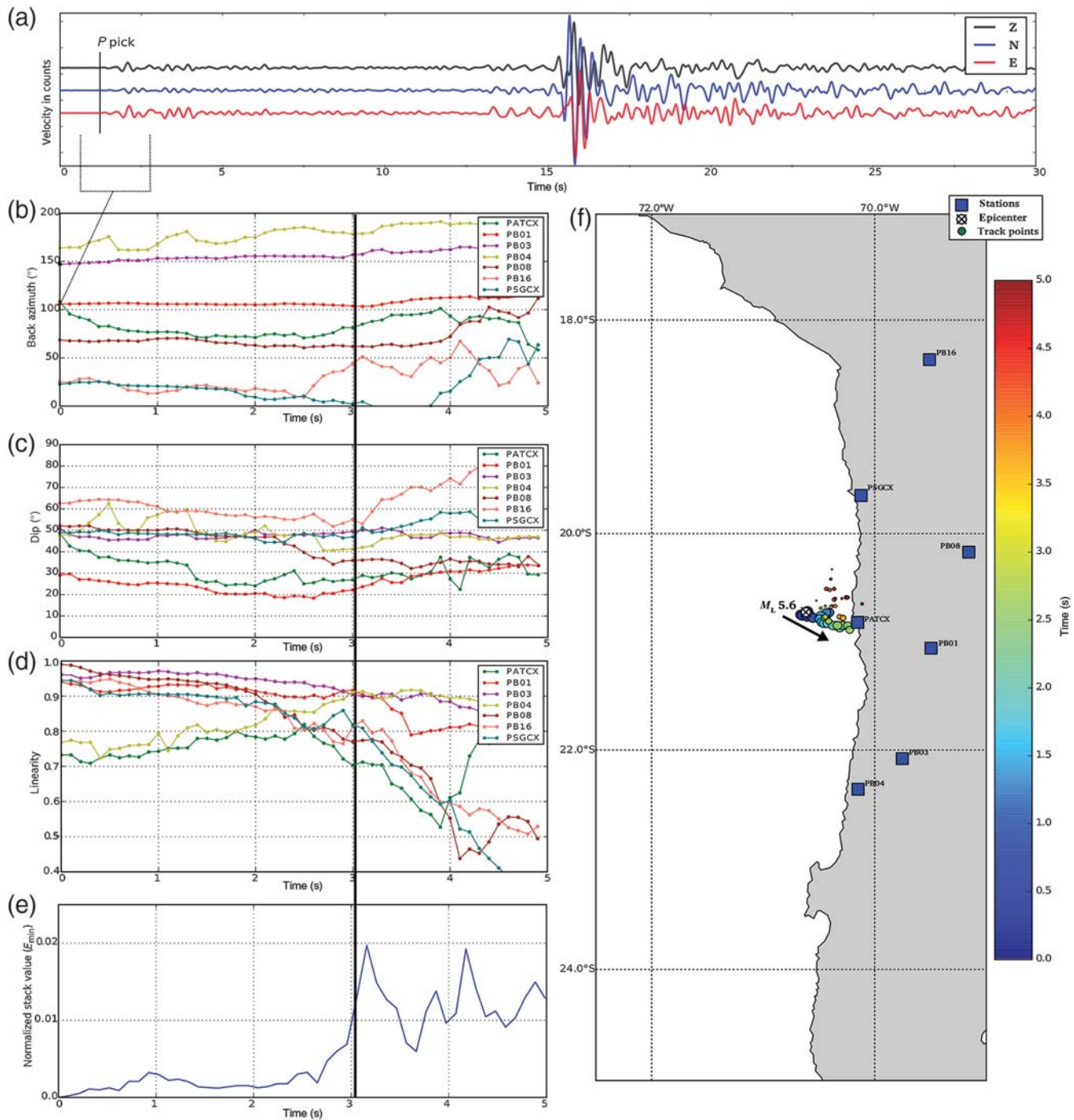
We illustrate the performance of the P -wave polarization-based method exemplarily for an M_L 5.6 event of 3 April 2014. Figure 3 shows the seismogram at one station, PB01, and the back-azimuth estimates for all stations as a function of time for a 5-s time interval of the P -wave coda (Fig. 3b).

The procedure works as follows: first, waveforms are band-pass filtered from 0.5 to 5 Hz. Then, the back-azimuth values of the P -phase onset are estimated using a sliding time window of 250 samples. The obtained values are visualized in horizontal particle-motion hodograms (⊕ Fig. S1, available in the electronic supplement to this article). The time window length is chosen empirically such that it produces back-azimuth curves that are stable, without short-term fluctuations, and it is still small enough to resolve directivity for events with rupture duration in the order of only a few seconds.

Second, the obtained back-azimuth estimates at P -onset time are used to select stations where the wavefield polarity is close to the back azimuth of the connecting line between receiver and known epicenter. We allow a maximal deviation of 15° assuming that a static offset in back azimuth does not influence the time-dependent variation of the measured polarization at the station. This deviation may be caused, for example, by lateral heterogeneity of the local velocity structure. Stations are then statically corrected such that the first back-azimuth estimates point exactly to the epicenter (illustrated in ⊕ Fig. S2). In addition to the weighting by linearity, we apply geometrical weighting.

Based on the event location, stations are weighted according to their location in eight equally weighted azimuth sectors of 45° . The procedure ensures a tolerably even contribution of observations from different angles. For each timestep, the stacking points are plotted onto the map at the location of E_{\min} . This is called the rupture track. The curve in Figure 3c illustrates the time evolution of the deviation stack value E_{\min} , which is a measure of coherency of the back-azimuthal directions. The sharp increase of E_{\min} at about 3 s indicates the end of the rupture propagation, where radiation of seismic energy stops, linearity at all stations decreases, and incoherent back azimuths are obtained. In the map view in Figure 3f, this is illustrated by a decreasing size of the tracking points. We show the analysis for a time window of 5 s, which is sufficient to comprise the rupture duration for most of the events within our catalog (Bilek *et al.*, 2004).

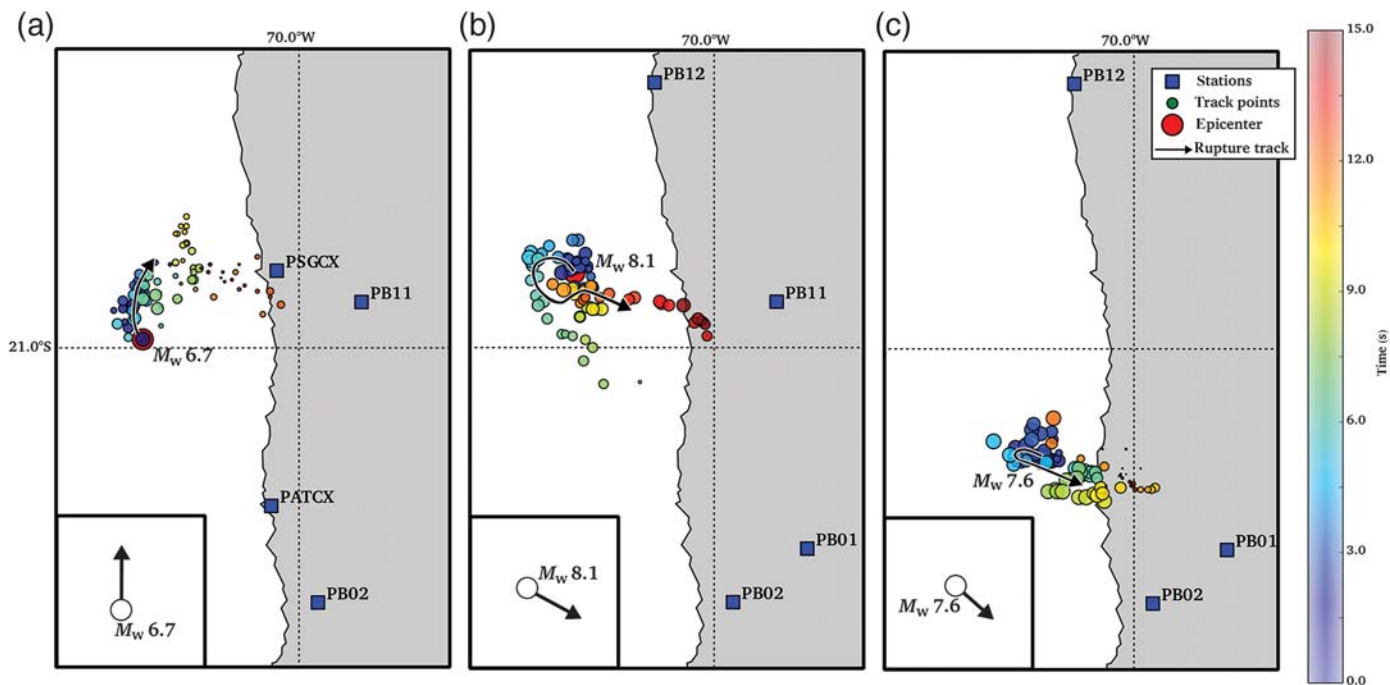
In the last step, we routinely use different time windows (1, 2.5, and 5 s) to compute averaged directions between the track locations and the epicenter. By careful visual inspection, the best-fitting window is found and the rupture direction is determined.



▲ **Figure 3.** (a) Three-component waveform of the 3 April M_L 5.6 event at station PB01; (b) back azimuth versus time for seven stations for a time window of 5 s; (c) corresponding dip estimates; (d) linearity values; and (e) the normalized deviation stack E_{min} . Note that stations with stronger short-term fluctuations in back azimuth show generally lower linearity values. The value of E_{min} increases abruptly at about 3 s, indicating a stop of rupture. (f) Resulting track of the rupture. The tracking points are color coded with progressing time from blue to red. Rupture direction is stable for the first 3 s and oriented $\sim 118^\circ$ from north.

The M_L 5.6 earthquake of 3 April 2014 exhibits a clear and consistent rupture track indicating a unilateral propagation toward 118° from north. The east-southeast-directed rupture trend is already visible in the back-azimuth plots. Station PSGCX to the north of the epicenter shows decreasing back-

azimuth values with time, whereas station PB03 to the south exhibits increasing values. Station PB01, which is located approximately in the direction of the rupture propagation, has a consistent and constant back-azimuth value of about 115° , which in this case nicely constrains the rupture direction.



▲ **Figure 4.** Tracks of (a) the 2014 M_w 6.7 foreshock, (b) the M_w 8.1 mainshock, and (c) the M_w 7.6 aftershock derived from P -wave polarization of the local IPOC recordings for the first 15 s of the ruptures. The black arrows follow the main trend of the rupture propagation. The insets in the lower left corners indicate inferred rupture directions for the early rupture phases imaged by teleseismic back-projection (Meng *et al.*, 2015, see their fig. 1). The results are in reasonable agreement.

Station PATCX indicates a somewhat different direction; however, it has poor linearity and is down-weighted accordingly (compare to equation 1).

The two main pieces of information from the rupture track are (1) the observation of a primarily unilateral onset of rupture and (2) the rupture direction during that time. Because we apply time averaging, which is inherently a temporal and spatial smoothing at once, we interpret only the overall direction of the rupture track. In case of large events, we can only analyze the early phase of the rupture, as the S - P time window might be too short to capture the entire duration of the radiated P wave. For small events, shorter sliding time windows would be necessary, which, however, cannot be used due to decreasing stability of the back-azimuth estimation process. The rise of the deviation stack value is only a proxy for the source duration because it is also affected by the choice of the sliding time window.

TEST

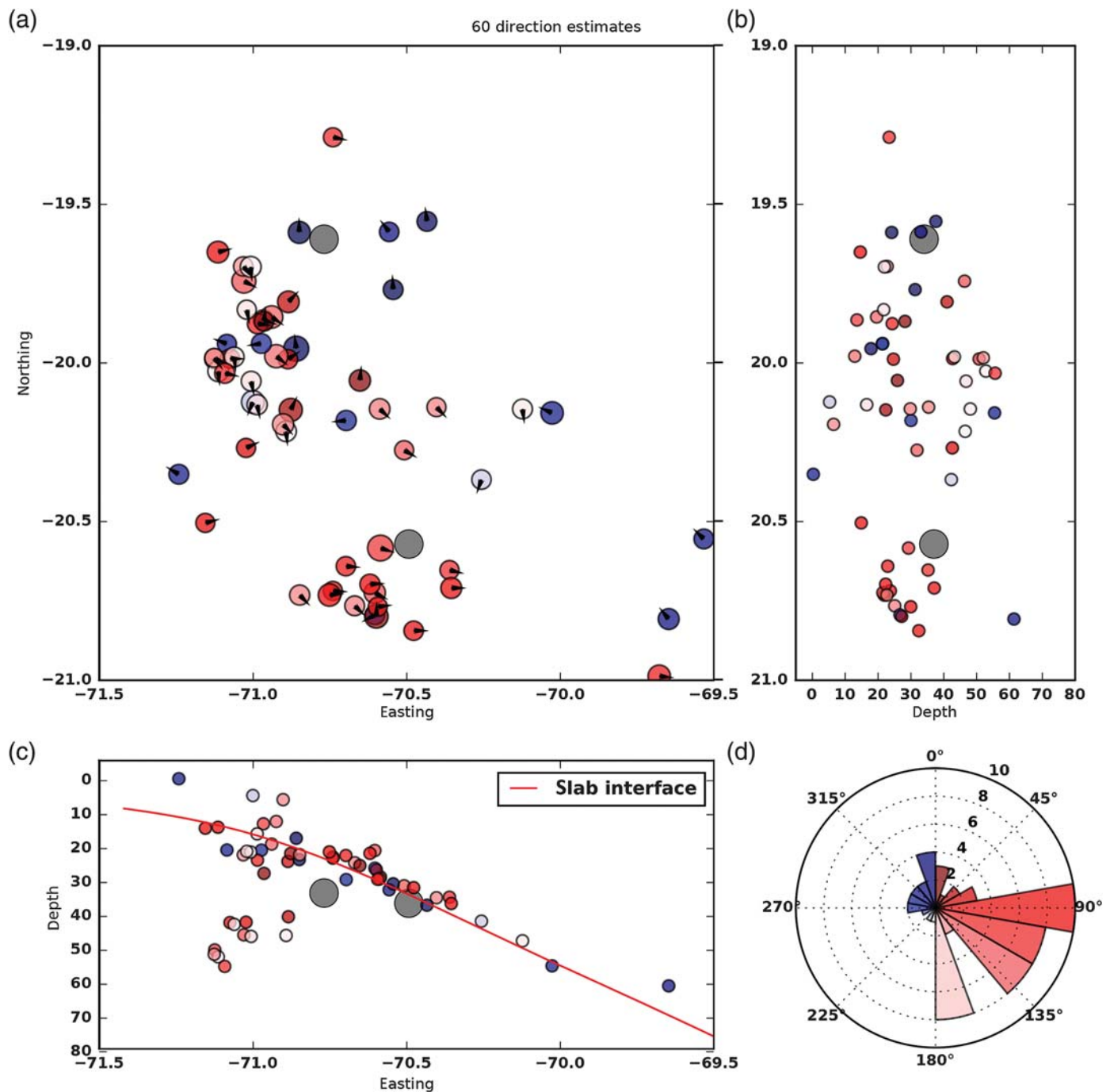
Our methodology is tested for the 2014 M_w 8.1 Iquique earthquake, the M_w 6.7 foreshock, and the M_w 7.6 aftershock, that have previously been imaged by teleseismic back-projection (Schurr *et al.*, 2014; Meng *et al.*, 2015). Figure 4 displays the polarization-analysis-based rupture tracks for the three events. For comparison, main rupture trends inferred from the back-projection images reported in Meng *et al.* (2015) are shown in insets.

A general consistency of the rupture directions from both approaches can be observed; that is, the main rupture trends are imaged similarly in all three cases. In particular, for the M_w 6.7 event the northward directed rupture is imaged concordantly by both approaches. Although the teleseismic imaging can cover the entire rupture process of the $M > 7$ earthquakes, the polarization-based local approach is limited to the first in our configuration ~ 15 s of the rupture due to the interference of the P -wave coda with the incoming S wave. On the other hand, the analysis of the local data provides a more detailed picture of the early rupture phase of the larger earthquakes. For example, the M_w 8.1 main event seems to break initially in up-dip direction and then turns in down-dip east-southeast direction after a few seconds.

These smaller scale features suggest the potential to image smaller magnitude events with the polarization-analysis-based approach.

RESULTS AND DISCUSSION

Analogously, we applied the P -wave polarization analysis to the 146 $M \geq 5$ events within the data catalog for the years 2013 and 2014. For 60 out of them, we are able to determine the rupture directions. We illustrate exemplary results in © Figures S3 and S4. We interpret the rupture behavior of these events as preferentially unilateral and obtain estimates of their rupture directions which are summarized in Figure 5 (compare to © Table S1). The remaining events may feature a more



▲ **Figure 5.** (a) Map and (b,c) depth sections of obtained rupture directions for the 60 $M \geq 5.0$ earthquakes. (d) Symbols are color coded by back azimuth according to the rose diagram. The two large gray circles are the M_w 8.1 main event and the M_w 7.6 aftershock. The red line in (c) marks the plate interface (Slab 1.0, Hayes *et al.*, 2012). Note the dominance of eastward (down-dip) rupture directions.

complex rupture behavior, for example, preferentially bilateral or circular ruptures, changes in rupture direction, or jumps of the areas of maximum seismic energy release. It is evident that for events with more complex rupture patterns, the method is not well suited.

Figure 5 shows the spatial distribution of the 60 obtained rupture directions in (a) map and (b,c) side view with a color coding corresponding to the rose diagram (d). We find a pre-

dominance of rupture directivity toward east, southeast, and south. Only very few events show directivity toward southwest, west, northwest, or north.

The directions of the $M \geq 5$ events reflect the rupture directivity obtained for the large M_w 8.1 and 7.6 events. Especially for the M_w 7.6 earthquake, many aftershocks close to its rupture area are found to point in a similar direction. They are mostly located directly on or close to the plate

interface. Moment tensor inversion shows a great conformity of fault-plane solutions, with the vast majority of events having shallow thrust mechanisms with the fault plane parallel to the slab interface (Cesca *et al.*, 2016). The here-observed uniform pattern of rupture directivity is in agreement with this finding.


CONCLUSIONS

The high-quality data and low noise conditions of the IPOC broadband seismic network are the prerequisite for accurate measurements of the P -wave polarization for local subduction earthquakes in northern Chile. We use this precondition and apply a polarization-based rupture tracking method to the seismic sequence of the M_w 8.1 Iquique earthquake. The method provides reasonably consistent results with teleseismic rupture backprojection imaging for the largest three earthquakes, that is, the 2014 M_w 8.1 mainshock, the M_w 6.7 foreshock, and the M_w 7.6 aftershock.

The great benefit of the method is the applicability to smaller sized earthquakes, in our case to events with magnitudes $M \geq 5.0$. In total, 60 of the studied $M \geq 5.0$ subduction earthquakes show clear unilateral behavior, and their rupture directions can be determined. These are preferentially oriented toward east, that is, in down-dip direction.

The demonstrated feasibility of the method using local seismic network data may in the future provide more detailed information, particularly of the first seconds of the rupture processes of large earthquakes than can be obtained by teleseismic backprojection.

DATA AND RESOURCES

Seismograms used in this study were recorded by the seismic CX-net of the Integrated Plate boundary Observatory Chile (IPOC, 2006) using STS-2 broadband seismometers. Data were obtained from the European Integrated Data Archive (EIDA)/GEOPHONE webpage (eida.gfz-potsdam.de/webdc3/ or geofon.gfz-potsdam.de/waveform/, last accessed September 2017). Picks, magnitudes, and event hypocenter were taken from a currently not yet publicly accessible catalog by Sippl and Schurr (2017). Data processing and figure production was mainly performed using Python3.5.1 (python.org, last accessed September 2017) and packages IPython4.2.0 (Pérez and Granger, 2007), NumPy (Walt *et al.*, 2011), Matplotlib (Hunter, 2007), and ObsPy (Beyreuther *et al.*, 2010). Some figures were produced and/or refined using Inkscape (inkscape.org, last accessed September 2017). 

ACKNOWLEDGMENTS

J. F. was funded by the German Science Foundation, DFG, Project Number SH 55/15-1. The authors greatly appreciate the constructive comments from the editors and our anonymous reviewers who helped us increase the quality of the article. The authors thank the developers and communities of the utilized open source resources (compare to [Data and Resources](#))

and the authors thank all institutions that are involved with operating the Integrated Plate boundary Observatory Chile (IPOC) network.

REFERENCES

- Bayer, B., R. Kind, M. Hoffmann, X. Yuan, and T. Meier (2012). Tracking unilateral earthquake rupture by P-wave polarization analysis, *Geophys. J. Int.* **188**, no. 3, 1141–1153.
- Beyreuther, M., R. Barsch, L. Krischer, T. Megies, Y. Behr, and J. Wassermann (2010). ObsPy: A Python toolbox for seismology, *Seismol. Res. Lett.* **81**, no. 3, 530–533.
- Bianchi, M., P. L. Evans, A. Heinloo, and J. Quinteros (2015). *Webdc3 Web Interface, GFZ Data Services*, doi: [10.5880/GFZ.2.4/2016.001](https://doi.org/10.5880/GFZ.2.4/2016.001).
- Bilek, S., T. Lay, and L. Ruff (2004). Radiated seismic energy and earthquake source duration variations from teleseismic source time functions for shallow subduction zone thrust earthquakes, *J. Geophys. Res.* **109**, no. B9, doi: [10.1029/2004JB003039](https://doi.org/10.1029/2004JB003039).
- Bürgmann, R. (2014). Warning signs of the Iquique earthquake, *Nature* **512**, no. 7514, 258.
- Calderoni, G., A. Rovelli, Y. Ben-Zion, and R. Di Giovambattista (2015). Along-strike rupture directivity of earthquakes of the 2009 L'Aquila, central Italy, seismic sequence, *Geophys. J. Int.* **203**, no. 1, 399–415.
- Cesca, S., F. Grigoli, S. Heimann, T. Dahm, M. Kriegerowski, M. Sobiesiak, C. Tassara, and M. Olcay (2016). The M_w 8.1 2014 Iquique, Chile, seismic sequence: A tale of foreshocks and aftershocks, *Geophys. J. Int.* **204**, no. 3, 1766–1780.
- Comte, D., and M. Pardo (1991). Reappraisal of great historical earthquakes in the northern Chile and southern Peru seismic gaps, *Nat. Hazards* **4**, no. 1, 23–44.
- Folesky, J., J. Kummerow, and S. Shapiro (2013). Rupture propagation imaging at microseismic scale, *75th EAGE Conf. and Exhibition Incorporating SPE EUROPEC 2013*, London, United Kingdom, 10–13 June 2013.
- Hayes, G. P., M. W. Herman, W. D. Barnhart, K. P. Furlong, S. Riquelme, H. M. Benz, E. Bergman, S. Barrientos, P. S. Earle, and S. Samsonov (2014). Continuing megathrust earthquake potential in Chile after the 2014 Iquique earthquake, *Nature* **512**, no. 7514, 295.
- Hayes, G. P., D. J. Wald, and R. L. Johnson (2012). Slab1.0: A three-dimensional model of global subduction zone geometries, *J. Geophys. Res.* **117**, no. B1, doi: [10.1029/2011JB008524](https://doi.org/10.1029/2011JB008524).
- Hunter, J. D. (2007). Matplotlib: A 2D graphics environment, *Comput. Sci. Eng.* **9**, no. 3, 90–95.
- Integrated Plate boundary Observatory Chile (IPOC) (2006). *IPOC Seismic Network. Integrated Plate boundary Observatory Chile - IPOC*, GFZ German Research Centre for Geosciences; Institut des Sciences de l'Univers-Centre National de la Recherche CNRS-INSU, Seismic Network, doi: [10.14470/PK615318](https://doi.org/10.14470/PK615318).
- Ishii, M., P. M. Shearer, H. Houston, and J. E. Vidale (2005). Extent, duration and speed of the 2004 Sumatra–Andaman earthquake imaged by the Hi-Net array, *Nature* **435**, no. 7044, 933.
- Jurkevics, A. (1988). Polarization analysis of three-component array data, *Bull. Seismol. Soc. Am.* **78**, no. 5, 1725–1743.
- Kato, A., and S. Nakagawa (2014). Multiple slow-slip events during a foreshock sequence of the 2014 Iquique, Chile M_w 8.1 earthquake, *Geophys. Res. Lett.* **41**, no. 15, 5420–5427.
- Krüger, F., and M. Ohrnberger (2005). Spatio-temporal source characteristics of the 26 December 2004 Sumatra earthquake as imaged by teleseismic broadband arrays, *Geophys. Res. Lett.* **32**, no. 24, doi: [10.1029/2005GL023939](https://doi.org/10.1029/2005GL023939).
- Meng, L., H. Huang, R. Bürgmann, J. P. Ampuero, and A. Strader (2015). Dual megathrust slip behaviors of the 2014 Iquique earthquake sequence, *Earth Planet. Sci. Lett.* **411**, 177–187.
- Pérez, F., and B. E. Granger (2007). IPython: A system for interactive scientific computing, *Comput. Sci. Eng.* **9**, no. 3, doi: [10.1109/MCSE.2007.53](https://doi.org/10.1109/MCSE.2007.53).

- Rentsch, S., S. Buske, S. Lüth, and S. Shapiro (2006). Fast location of seismicity: A migration-type approach with application to hydraulic-fracturing data, *Geophysics* **72**, no. 1, S33–S40.
- Ruiz, S., M. Metois, A. Fuenzalida, J. Ruiz, F. Leyton, R. Grandin, C. Vigny, R. Madariaga, and J. Campos (2014). Intense foreshocks and a slow slip event preceded the 2014 Iquique M_w 8.1 earthquake, *Science* **345**, no. 6201, 1165–1169.
- Schurr, B., G. Asch, S. Hainzl, J. Bedford, A. Hoechner, M. Palo, R. Wang, M. Moreno, M. Bartsch, Y. Zhang, *et al.* (2014). Gradual unlocking of plate boundary controlled initiation of the 2014 Iquique earthquake, *Nature* **512**, no. 7514, 299.
- Sippl, C., and B. Schurr (2017). Anatomy of a subduction zone—Seismicity structure of the northern Chilean forearc from > 100,000 double-difference relocated earthquake hypocenters, *EGU General Assembly Conf. Abstracts, Volume 19 of EGU General Assembly Conf. Abstracts*, 5466.
- Socquet, A., J. P. Valdes, J. Jara, F. Cotton, A. Walpersdorf, N. Cotte, S. Specht, F. Ortega-Culaciati, D. Carrizo, and E. Norabuena (2017). An 8 month slow slip event triggers progressive nucleation of the 2014 Chile megathrust, *Geophys. Res. Lett.* **44**, no. 9, 4046–4053.
- Tinti, E., L. Scognamiglio, A. Michelini, and M. Cocco (2016). Slip heterogeneity and directivity of the M_L 6.0, 2016, Amatrice earthquake estimated with rapid finite-fault inversion, *Geophys. Res. Lett.* **43**, no. 20, 10,745–10,752.
- Walt, S. v. d., S. C. Colbert, and G. Varoquaux (2011). The NumPy array: A structure for efficient numerical computation, *Comput. Sci. Eng.* **13**, no. 2, 22–30.

J. Folesky
J. Kummerow
S. A. Shapiro
Freie Universität Berlin
Department of Geophysics
Malteser Street 74-100
12249 Berlin, Germany
jonas.folesky@geophysik.fu-berlin.de

G. Asch
B. Schurr
Ch. Sippl
*F. Tilmann*¹
Helmholtz-Zentrum Potsdam
Deutsches GeoForschungsZentrum GFZ
Telegrafenberg
14473 Potsdam, Germany

¹ Also at Freie Universität Berlin, Department of Geophysics, Malteser Street 74-100, 12249 Berlin, Germany.